Fixed-Structure Parameter-Dependent State Feedback Controller: an Scaled Autonomous Vehicle Path-Tracking Application

Ariel Borrell, Vicenç Puig, Olivier Sename

Fixed-Structure Parameter-Dependent State Feedback Controller: an Scaled Autonomous Vehicle Path-Tracking Application

Ariel M. Borrell[a,b], Vicenç Puig[a], Olivier Sename[b]

[a]*Institut de Robòtica i Informàtica Industrial (CSIC-UPC), C/. Llorens i Artigas 4-6, Barcelona, 08028, Spain*
[b]*Univ. Grenoble Alpes, CNRS, Grenoble INP, GIPSA-Lab, Grenoble, 38000, France*

Abstract

This paper introduces theoretical conditions for the computation of a novel type of state-feedback controller that makes use of Linear Parameter Varying approaches for synthesis. The novelty of this new State-Feedback controller lies on the fact that the controller has a fixed structure with constants matrix gains. However, the controller gains are affine on a parameter dependent basis function, which allows the controller to self-schedule according to real-time changes of the varying parameters. This type of controller is conceived with a focus on implementation, as in contrast with most other LPV approaches. The implementation of this Parameter-Dependent State-Feedback controller does not require any online interpolation or matrix inverse operations, independently of the number of varying parameters. The performance of the proposed approach is validated in a Scaled Autonomous Vehicle for steering control in a path tracking application.

Keywords: LPV, Robust Control, Parameter-Dependent Controller, Autonomous Vehicle, Lateral Dynamics

1. Introduction

In this paper, we introduce a simple to implement Linear Parameter Varying (LPV) controller with fixed structure but depending on some time-varying parameters. In the following subsection, we describe the most well known LPV methods, e.g Polytopic and Grid based approaches, to explore their trade-off, both from a robustness and stability guarantees and from their implementation complexity perspectives. Then, we define the control problem for this new type of LPV controllers followed by a description of the paper objectives and contributions.

1.1. Literature review

The LPV approach (Shamma, 2012) is nowadays a well-established approach in the literature. Part of the success of the LPV framework comes from its ability to capture the dynamics of complex non-linear system as a time-varying linear system thanks to the use of scheduling parameters. This enables the use of Linear Matrix Inequalities (LMI) based LTI control techniques (Boyd et al., 1994) as a basis for the control and analysis solution for non-linear systems, while providing performance and robustness guarantees. From an implementation point of view, the practical implementation of LPV controllers depends on the approach used for synthesis, with the most popular synthesis approaches being the Polytopic and Grid based approaches. A brief introduction of each approach is given in the following.

The Polytopic approach assumes a finite family of LTI systems whose convex combination covers the behaviour of the LPV system (López-Estrada et al., 2019). In this way, defining the synthesis conditions on the vertices of this convex bounding polytope guarantees stability and performance for all points inside the polytopic region of the varying parameters. These strong guarantees are achieved by making use of a common Lyapunov function for all vertices with shared constant positive definite Lyapunov matrix (Apkarian et al., 1995). Although theoretically strong, this approach in practice is often conservative as usually the parameter space is over bounded by the convex polytopic region, which may lead to vertices with parameter combination which are not physically feasible. This issue has been tackled in a number of works on proposed algorithms for polytope size reduction, e.g. (Kwiatkowski and Werner, 2008; Hoffmann et al., 2012; Rizvi et al., 2016; Sanjuan et al., 2022), or on the use of ad-hoc methods for polytope reduction for some specific systems as in (Baldelli et al., 2008; Kapsalis et al., 2022).

The other distinctive source of conservatism in the

Polytopic approach is the use of a constant positive-definite matrix in the common Lyapunov function of the LPV system. In the case of Discrete-Time LPV (DT LPV) systems, this issue has been solved with the introduction of the Poly-Quadratic Lyapunov Function (Daafouz and Bernussou, 2001a,b). The synthesis conditions introduced in these works make use of a type of Parameter-Dependent Lyapunov Functions (PDLF) such that a unique positive-definite Lyapunov matrix is defined at each polytope vertex. In addition, these conditions make use of the additional slack variable G introduced in (de Oliveira et al., 1999). This new slack variable allows to decouple the Lyapunov matrix from the standard change of variable associated with the controller gain, which alleviate the Lyapunov matrix from extra constraints. The use of this new slack variable is referred to as G-shaping paradigm (Oliveira et al., 2002). Overall, this G-shaping paradigm in addition to Poly-Quadratic Lyapunov Function offers many advantages in terms of reduction of conservatism when compared with the standard Polytopic approach. Despite these improvements, there is still another important source of conservatism that both Poly-Quadratic and traditional Polytopic methods share. The use of a constant Lyapunov matrix, or a polytopic set of constant Lyapunov matrices in the Poly-Quadratic case, represents that the varying parameter can change in value arbitrarily fast, something which is extremely conservative and in fact is not suitable for some systems (Wu et al., 1996).

The Grid based approach is the most similar to the traditional "gain-scheduling" approach for non-linear systems, since the LPV model is obtained as a set of LTI systems defined alongside the trajectory of the scheduling functions evaluated at fixed values of the varying parameters (Wu et al., 1996). During the synthesis step, it is commonly considered affine Parameter Dependent Lyaounov Matrices (PDLM), with the so-called basis functions that form the affine PDLM being an important decision to be made by the control designer (Apkarian and Adams, 1998). An important consequence of using such Lyapunov functions with parameter dependency is that Grid based methods can account for limits on the rate of variation for the varying parameters.

By using a set of LTI models over frozen points of the scheduling variables space, the induced issue of over bounding by the Polytopic approach is avoided. Together with the use of PDLF and limits on the rate of variation for the varying parameters means that the Grid-based approach allows to alleviate much of the conservatism that is associated with the Polytopic method. However, this is achieved with the trade-off that there is no strong guarantees outside of the frozen values on the scheduling space that were considered for synthesis. For this reason, it is recommended very dense grids of frozen values on the parameter space. However, this is usually difficult to achieve due to computational limitations. Moreover, the need for a dense grid for the synthesis of robust Grid based LPV controllers requires in practice a large family of pointwise LTI controllers to be implemented, a larger family of LTI controllers than an equivalent Polytopic design would require. A common approach to alleviate this implementation issue is to carry out the synthesis of Grid based LPV controllers on a first grid, and check if the performance of the closed-loop still holds on a much tighter grid in a second step (Becker, 1996). Alternatively, recent stability analysis results introduced in (Cox et al., 2018) could be used as a substitute for this second step.

All these families of modelling and synthesis approaches for LPV systems, with their advantages and disadvantages, have been successfully applied in many works including experimental validation in some of them (see (Mohammadpour and Scherer, 2012; Hoffmann and Werner, 2015; Liu et al., 2018; Li et al., 2021; Hang and Chen, 2021; Corno et al., 2021; Atoui et al., 2022) and references therein). Notably, in (Atoui et al., 2022) LPV approaches are compared in an experimental setup for the lateral control of an autonomous vehicle. The authors of this work concluded that the Polytopic approach can be too conservative for some ranges of the parameter space, meanwhile the Grid based approach showed quite robust performances.

1.2. Motivation

Although successfully validated, and clearly better than pure robust LTI approaches (Kajiwara et al., 1999), the LPV approach can suffer from practical difficulties during implementation, particularly when the complexity of the controlled system increases. The Polytopic method requires 2^n controllers to be computed and implemented, n being the number of vertices for the convex polytope. Similarly, in the Grid based approach the number of point-wise controllers increases exponentially with the number of frozen values of the varying parameters (remember that it is recommended a quite dense grid in order to obtain robustness guarantees). It can be easily seen how for the Polytopic and Grid-based approaches the amount of point-wise controllers to be implemented and stored in memory quickly increases in number as the complexity of the system increases.

These issues are in part the main motivation of works in the Polytopic approach for vertex reduction, which have been commented before. Also it has led to some

works that seek explicitly to reduce and address the complexity of implementation of the obtained controller after synthesis (Hoffmann et al., 2014; Bianchi and Sánchez-Peña, 2022; Sato, 2022). Clearly the practical implementation of LPV controllers is still a subject which deserves great attention in order to enable the widespread use of LPV techniques.

On the other hand, comparing approaches for LPV synthesis conditions, the least conservative synthesis conditions for LPV systems are those introduced for DT LPV systems with the G-Shaping paradigm, specially those introduced in (Pandey and de Oliveira, 2019). However, in the LPV literature the G-Shaping is used exclusively for Polytopic LPV systems, which induce conservatism due to over bounding of the parameter space and the assumption on an infinitely fast rate of varying parameter change. To the best of the author knowledge no work has extrapolated the use of G-Shaping like conditions for DT LPV Grid based approaches.

For these reasons, the main motivation of this work is to propose a new LPV approach that can be easily implementable, and whose synthesis makes use of the less conservative G-Shaping conditions in a DT Grid based approach. The control problem formulation for this new type of controllers is given in the following subsection.

1.3. Notation

The vector and matrix notation is standard. $\|\cdot\|_2$ represents the L_2-norm. x^T represents the transpose of x. X^{-1} represents the inverse of X, matrix $X > 0$ represents that X is symmetric positive-definite, $\mathcal{X} = ker(X)$ represents that $\mathcal{X}$ is a base of the null space of X, the notation $\text{He}(X) = X + X^T$ and $\star$ in an LMI represents a symmetric element transposed. In LMI given during theorems or propositions, bold letters $\mathbf{X}$ are used to identify the matrix X as an optimization variables in the LMI problem.

The following notation is used in the description of DT-LPV systems. For simplification, the time dependency on the varying parameter vector $\rho(k)$ will be dropped, e.g. $\rho := \rho(k)$, unless it is required for clarification. Subscript i indicates that it is being referred to an individual element ρ_i of a varying parameter vector ρ. Superscript + indicates that a time dependent vector $x(k)$ or parameter dependent matrix $X(\rho(k))$ is being evaluated at time instance $k+1$, e.g. $x^+ := x(k+1)$ and $X^+ := X(\rho(k+1))$. Subscript p will represent that a parameter dependent vector $x(\rho)$ or matrix $X(\rho)$ is evaluated at a frozen grid-point g_p, e.g. $x_p := x(g_p)$. When considering a polytope around a frozen grid-point g_p, the superscript v indicates that a parameter vector $x(\rho)$ or a parameter dependent matrix $X(\rho)$ is evaluated at a vertex g_p^v of such polytope, e.g. $x_p^v := x(g_p^v)$ and $X_p^v := X(g_p^v)$.

1.4. Control Problem Definition

This paper is concerned with DT-LPV systems of the form:

$$\Xi(\rho) := \begin{cases} x^+ = A(\rho)x + B_u(\rho)u + B_w(\rho)w \\ z = C_z(\rho)x + D_u(\rho)u + D_w(\rho)w \end{cases} \tag{1}$$

where $x \in \mathbb{R}^{n_x}$ is the state vector, $u \in \mathbb{R}^{n_u}$ are the control inputs, $w \in \mathbb{R}^{n_w}$ are the exogenous inputs with bounded energy such that $w \in L_2$ and $z \in \mathbb{R}^{n_z}$ are the exogenous outputs.

$\rho := (\rho_1, \ldots, \rho_m)^T$ is a vector with m varying parameters, $\rho_i \in \mathbb{R}$. The range of values of each individual varying parameter ρ_i and its rate of variation ν_i are satisfying the following assumptions:

- Each varying parameter ρ_i is measured online, e.g. at a time instant k the value of $\rho(k)$ is known, and bounded by extremal values $\underline{\rho}_i$ and $\overline{\rho}_i$ such that $\underline{\rho}_i \leq \rho_i(k) \leq \overline{\rho}_i$. These bounds on ρ then form the varying parameter admissible space $\Omega \in \mathbb{R}^m$, such that $\forall k$ then $\rho(k) \in \Omega$.
- The rate of variation ν_i of each varying parameter ρ_i between two consecutive sampling times k and $k+1$ is not necessarily available online, however, the maximum variation rates are known and bounded by $\underline{\nu}_i$ and $\overline{\nu}_i$ such that $\forall k$ then $\underline{\nu}_i \leq \nu_i(k) \leq \overline{\nu}_i$.

The parameter dependency for each of the state space matrix of $\Xi(\rho)$ is assumed to be given by an affine relation with a scheduling signal $\theta(\rho)$ as (Apkarian and Adams, 1998; Cox et al., 2018):

$$A(\rho) = A_0 + \sum_{n=1}^{N} \theta_n(\rho) A_n, \tag{2}$$

where

$$\theta(\rho) := (1, \theta_1(\rho), \ldots, \theta_N(\rho)), \tag{3}$$

forms the so-called basis functions, and $\theta_n(\rho) \in \mathbb{R}$ is a linear or nonlinear function.

The control problem introduced in this paper is given in the framework of $\mathcal{H}_\infty/LPV$ control making use of the Induced L_2-norm, which is defined as follows:

Definition 1 (Induced L_2-norm (Boyd et al., 1994))**.** *The induced L_2-norm of a system is the quantity*

$$\sup_{\|w\|_2 \neq 0} \frac{\|z\|_2}{\|w\|_2}, \tag{4}$$

where the L_2-norm of u is $\|u\|_2^2 = \int_0^\infty u^T u dt$.

Within the $\mathcal{H}_\infty/LPV$ framework, our objective is to find a Parameter-Dependent State-Feedback (PDSF) controller with a fixed structure, which is defined as follows:

Definition 2 (Parameter-Dependent State-Feedback Controller)**.** *The structure of the PDSF Controller is defined as follows:*

$$K(\rho) = K_0 + \sum_{n=1}^{N} \theta_n(\rho) K_n \,, \tag{5}$$

where the controller gains $K_0, \ldots, K_N$ are constant matrices, $\theta(\rho)$ is the scheduling function defined in (3)*.*

The PDSF synthesis problem is then posed as the minimization of the induced L_2-norm of a closed-loop LPV system. Such control problem is given in the following definition.

Definition 3 (PDSF Induced L_2-norm Control Problem)**.** *Given an LPV system $\Xi(\rho)$ and considering an State-Feedback control law $u = K(\rho)x$, the resulting LPV closed-loop system is:*

$$\Xi_{CL}(\rho) := \begin{cases} x^+ = (A(\rho) + B_u(\rho)K(\rho))x + B_w(\rho)w \\ z = (C_z(\rho) + D_u(\rho)K(\rho))x + D_w(\rho)w \end{cases} \tag{6}$$

Considering the induced L_2-norm of a system, given in Definition 1, the control problem is then to find a PDSF controller $K(\rho)$ according to Definition 2 that renders the LPV closed-loop system Ξ_{CL} robustly stable and minimizes its L_2-norm as:

$$\min_{\mathbf{K}(\rho), \gamma_\infty} \gamma_\infty \; s.t. \; \frac{\|z\|_2}{\|w\|_2} \leq \gamma_\infty \tag{7}$$

1.5. Paper Objectives and Contributions

Keeping in mind the implementability issues of LPV controllers, this paper introduces a new approach to design Linear Parameter Varying (LPV) State-Feedback (SF) controllers. The novelty of this new approach lies on the fact that the controller structure results directly from a chosen parametric dependency, similar as in the case of the basis function for PDLM (Wu et al., 1996; Apkarian and Adams, 1998). The fact that the controller gain matrices are constant for the whole LPV parameter space, makes this type of LPV controllers an extension of the robust control approach (de Oliveira et al., 1999; Rodrigues et al., 2018). Nonetheless, despite having fixed controller gains, the overall controller $K(\rho)$ is parameter dependent and can adapt online to the measured varying parameter values, which drastically reduces the conservatism associated with this solution.

To find an LPV controller whose structure is independent of the number parameter space grid points, the solution of the control synthesis problem is performed by solving two sequential LMI optimization problems. Similar as proposed for LFT LPV synthesis in (Apkarian and Gahinet, 1995), a first LMI problem is proposed as a feasibility LMI problem for the existence of general $\mathcal{H}_\infty$ controllers for a given control design, considering state-feedback controllers in this work. A second LMI problem then enables to reconstruct the controller gains. The key of this second step is that the controller gains $K_0, \ldots, K_n$ from $K(\rho)$ in Eq. (5) are the only decision variables.

As a result, the controller dimensions (in terms of the number of controller gains to be found and implemented) only depends on the size N of the scheduling basis function $\theta(\rho)$ and not on the number of frozen grid points values for the parameter space. This translates to an LPV state-feedback controller design which is straightforward to implement thanks to a reduced number of controller gains and as it does not requires any online interpolation.

Finally, in order to test the performance of the PDSF control method, it has been implemented into an Scaled Autonomous Vehicle (SAV) platform for the lateral control problem. Note that LPV approaches have been successfully applied for vehicle lateral dynamics control applications in the literature: in (Kapsalis et al., 2022) the authors implemented a Polytopic LPV controller in a test autonomous vehicle for steering control, the same vehicle platform was used in (Atoui et al., 2022) for a comparison of the LPV Polytopic, Griddding and Linear Fraction Transformation approaches, in (Li et al., 2022) the issue of actuator saturation in autonomous steering control is dealt using parameter dependent Lyapunov approaches, and, finally, (Alcalá et al., 2020) uses optimal control approaches in the LPV-MPC framework for the control problem in autonomous driving. In our application, the objective is to achieve robust path-tracking of a desired trajectory. In order to achieve this goal, the PDSF controller will act on the front servo motor of the SAV to autonomously steer the vehicle through a given track.

The contributions of this work can then be summarized as follows:

- Extension of the DT G-shaping paradigm conditions from the Polytopic approach (Oliveira et al., 2002) to a DT Grid based approach.
- Introduction of the PDSF controller synthesis con-

ditions for DT LPV systems.

- The PDSF synthesis leads to a simple to implement controller thanks to a reduced number of controller gains and does not requires online interpolation.
- Experimental validation of the PDSF controller for a path tracking application on an Scaled Autonomous Vehicle.

1.6. Paper Structure

The structure of the rest of the paper is the following. In Section 2, some preliminaries on the analysis of DT-LPV systems through LMI is given. In Section 3, new LMI conditions are introduced and used to prove the existence of the controller for a given system and numerical proposition for the computation of the PDSF controller gains. Section 4 describes the Scaled Autonomous Vehicle platform utilized for validation of the PDSF controller controller. Section 5 describes the synthesis approach for the path tracking application on the SAV while Section 6 presents the results. Finally, in Section 7, conclusions are drawn.

2. Preliminaries on the Analysis of Grid Based DT-LPV Systems

In this section, we introduce the framework employed to analyze through LMI the Grid based DT-LPV systems with the aid of Parameter Dependent Lyapunov Functions (PDLF). This framework and LPV related notation introduced in this section is employed for the derivation of results presented in following sections.

To discuss the stability concepts, it is considered here the autonomous DT-LPV system (obtained from (1)) and given by:

$$x^+ = A(\rho)x, \tag{8}$$

The parameter dependent state matrix $A(\rho)$ is represented by an affine relation on the scheduling function $\theta(\rho)$ (Apkarian and Adams, 1998; Cox et al., 2018):

$$A(\rho) = A_0 + \sum_{n=1}^{N} \theta_n(\rho) A_n, \tag{9}$$

where $\theta(\rho) := (1, \theta_1(\rho), \ldots, \theta_N(\rho))$ forms the so-called basis functions, $\theta_n(\rho) \in \mathbb{R}$ is a linear or nonlinear function.

In this work we consider quadratic PDLF of the type:

$$V(x, \rho) = x^T X(\rho) x, \tag{10}$$

where the Parameter-Dependent Lyapunov Matrix (PDLM) has the following structure:

$$X(\rho) = X_0 + \sum_{n=1}^{N} \theta_n(\rho) X_n \tag{11}$$

Considering a PDLF $V(x, \rho)$, it follows that the stability of the DT-LPV system (8) can be proved if the following condition is satisfied (Daafouz and Bernussou, 2001a):

$$V(x^+, \rho^+) - V(x, \rho) \leq 0, \tag{12}$$

Note that the structure of the PDLM copies that of the system matrix (2). Although this is not strictly required, this simple strategy has been proved effective (Wu et al., 1996; Apkarian and Adams, 1998).

Using a quadratic PDLF of the form (10) in condition (12) leads to the inequality

$$A^T(\rho) X(\rho^+) A(\rho) - X(\rho) \leq 0. \tag{13}$$

However, there exist two important issues with this condition. Firstly, condition (13) is an infinitely constrained LMI due to the infinite possible values ρ can take within its bound. Moreover, it involves both $\rho(k)$ and $\rho(k+1)$ and only $\rho(k)$ is known, with $\rho(k+1)$ generally unknown.

A common solution to the first issue is to consider a dense grid $\mathcal{G} \in \Omega$ at fixed ρ values and evaluate the stability condition at each grid-point $g_p \in \mathcal{G}$ (Wu et al., 1996). Despite considering a frozen grid of values for the varying vector ρ, it still remains an issue the fact that ρ^+ appearing in the stability condition (13) is unknown. However, knowing the information on the bounded variation rates ν_i, the parameter values at the new sample ρ_i^+ is limited within the range

$$\rho_i^+ \in \left[\rho_i - \underline{\nu}_i, \rho_i + \overline{\nu}_i\right] \tag{14}$$

This allows us to build, for each grid point $g_p \in \mathcal{G}$, a polytope which bounds the parameter variations at the next sample. This is specified for each varying parameter ρ_i ($g_{p,i}$ being the frozen value of ρ_i at the grid point g_p), with the min/max values :

$$\left[g_{p,i} - \underline{\nu}_i, g_{p,i} + \overline{\nu}_i\right], \forall i = 1, \ldots, m. \tag{15}$$

Overall this defines the bounding polytope $\mathcal{V}_p \in \Omega$ at each grid point $g_p \in \mathcal{G}$, where all the 2^m min/max combinations form the vertices of $\mathcal{V}_p$. The vertices of this polytope $\mathcal{V}_p$ are denoted $g_p^v \in \mathcal{V}_p$, with $v = 1, \ldots, 2^m$, in the remaining parts of the paper.

To better visualize this approach Fig. 1 is introduced. In

this figure it is represented a 2D gridded varying parameter space $\mathcal{G} \in \mathbb{R}^2$, and we will focus on a single grid point $g_p \in \mathcal{G}$. Knowing the parameter variation limits on ρ_1 and ρ_2, namely $(\underline{\nu}_1, \overline{\nu}_1)$ and $(\underline{\nu}_2, \overline{\nu}_2)$ respectively, then it is possible to build a local bounding polytyope $\mathcal{V}_p$ of 4 vertices such that $g_p^+ \in \mathcal{V}_p$. Notice that the order of the vertices g_p^v, $v = 1, \ldots, 4$, of $\mathcal{V}_p$ is not representative of any strict ordering requirement.

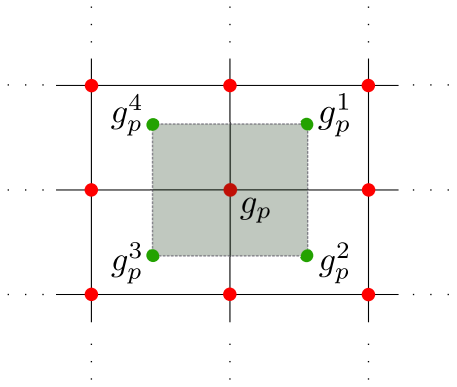

Figure 1: Vertices of the polytope $\mathcal{V}_p$ bounding g_p^+.

Applying this parameter grid and local variation bounds framework, it is then possible to recast condition (13) as a finite number of LMI independent of $X(\rho^+)$, but which bounds it locally at each $g_p \in \mathcal{G}$. Each LMI of the finite set of conditions is given $\forall(g_p, g_p^v)$ as:

$$A_p^T X_p^v A_p - X_p \leq 0, \forall v = 1, \ldots, 2^m. \tag{16}$$

Remark 1. *As $X(\rho^+)$ enters linearly on LMI* (13)*, there is only need to check the vertices of $\mathcal{V}_p \in \Omega$ to bound $X(\rho^+)$ around a fixed grid g_p (Apkarian and Adams, 1998). Thus, it suffice to replace $X(\rho^+)$ in LMI* (16) *by X_p^v for all (g_p, g_p^v) pairs.*

3. Synthesis Conditions for Parameter-Dependent State-Feedback Controllers with Fixed Structure

In this section the steps and conditions for the synthesis of PDSF controllers are given. In order to achieve the synthesis for this type of controllers, it is required a two-steps sequential LMI optimization problem procedure. The inspiration for this approach comes from the work of Apkarian and Gahinet (1995), in which a similar two-steps process was proposed for the computation of LFT LPV $\mathcal{H}_\infty$ controllers.

In a first step, we make use of the Projection Lemma over the Extended DT Bounded Real Lemma (BRL), see Lemma 2 in Appendix A.2, in order to obtain an LMI independent of the controller $K(\rho)$. At this first step, a feasible PDLM $X(\rho)$ and slack variable $G(\rho)$ are found as the decision variables on the LMI optimization Problem. In Sect. 3.1 and Sect. 3.2, general conditions and numerical propositions are given, respectively, to solve this first step LMI problem.

Using the numerical values for the PDLM $X(\rho)$ and $G(\rho)$, then the Extended DT BRL gives an LMI optimization problem where the only decision variable are the gains of $K(\rho)$, which has the structure considered in Eq. (5). In Sect. 3.3, we give numerical conditions to solve this problem and compute the gains for $K(\rho)$.

3.1. $\mathcal{H}_\infty$ State-Feedback Existence Conditions for DT-LPV Systems

It is considered here the DT-LPV system given previously in (1). The objective is to prove the existence of a SF LPV controller $K(\rho)$, such that the closed loop form of $\Xi(\rho)$ with feedback law $u = K(\rho)x$ is exponentially stable and with induced L_2-norm bounded by a scalar γ_∞ such that

$$\sup_{w(k)\neq 0} \frac{\|z(k)\|_2}{\|w(k)\|_2} \leq \gamma_\infty \tag{17}$$

The existence of such a controller, independent of its dependency on ρ, can be proved if the following theorem holds true.

Theorem 1. *Consider a DT-LPV system $\Xi(\rho)$ and scalar $\gamma_\infty > 0$. If, $\forall \rho \in \Omega$, there exist a symmetric positive-definite PDLM $X(\rho) \in \mathbb{R}^{n_x \times n_x}$, with fixed structure as in Eq.* (11)*, and a general slack matrix $\mathbf{G}(\rho) \in \mathbb{R}^{n_x \times n_x}$ such that the following condition holds:*

$$\mathcal{N}_M^T(\rho) \begin{bmatrix} \mathbf{G}^T(\rho) + \mathbf{G}(\rho) - X(\rho^+) & \star & \star & \star \\ A(\rho)G(\rho) & X(\rho) & \star & \star \\ C_z(\rho)G(\rho) & 0 & \gamma_\infty I & \star \\ 0 & B_w^T(\rho) & D_w^T(\rho) & \gamma_\infty I \end{bmatrix} \mathcal{N}_M(\rho) > 0 \tag{18}$$

with

$$X(\rho) = \mathbf{X_0} + \sum_{n=1}^{N} \theta(\rho)\mathbf{X_n}, \tag{19}$$

$$X(\rho^+) = \mathbf{X_0} + \sum_{n=1}^{N} \theta(\rho^+)\mathbf{X_n}, \tag{20}$$

$$\mathcal{N}_M(\rho) = ker\begin{bmatrix} 0 & B_u^T(\rho) & D_u^T(\rho) & 0 \end{bmatrix}, \tag{21}$$

then, there exists a SF control gain $K(\rho)$ such that the closed-loop form of $\Xi(\rho)$ is exponentially stable and γ_∞ is an upper bound on its induced L_2-norm, with control law given by $u = K(\rho)x$.

Proof: Consider a given positive scalar γ_∞ and given SF control law $u = K(\rho)x$, the closed-loop dynamics of $\Xi(\rho)$ are as follows:

$$\begin{aligned}\Xi_{CL}(\rho) &= \begin{cases} x^+ = (A(\rho) + B_u(\rho)K(\rho))x + B_w(\rho)w \\ z = (C_z(\rho) + D_u(\rho)K(\rho))x + D_w(\rho)w \end{cases} \\ &= \begin{cases} x^+ = \mathcal{A}(\rho)x + \mathcal{B}(\rho)w \\ z = C(\rho)x + \mathcal{D}(\rho)w \end{cases}\end{aligned} \tag{22}$$

where the following relations are used:

$$\begin{aligned} \mathcal{A}(\rho) &= A(\rho) + B_u(\rho)K(\rho) \quad \mathcal{B}(\rho) = B_w(\rho) \\ C(\rho) &= C_z(\rho) + D_u(\rho)K(\rho) \quad \mathcal{D}(\rho) = D_w(\rho) \end{aligned} \tag{23}$$

$\Xi_{CL}(\rho)$ is exponentially stable with induced L_2-norm less than γ_∞, if, according to Lemma 2 from Appendix A.2 the following sufficient condition is true:

$$\Psi(\rho,\rho^+) + \mathrm{He}\left(\begin{bmatrix} 0 \\ B_u(\rho) \\ D_u(\rho) \\ 0 \end{bmatrix} K(\rho) \begin{bmatrix} G(\rho) & 0 & 0 & 0 \end{bmatrix} \right) > 0 \tag{24}$$

where

$$\Psi(\rho,\rho^+) = \begin{bmatrix} G^T(\rho) + G(\rho) - X(\rho^+) & \star & \star & \star \\ A(\rho)G(\rho) & X(\rho) & \star & \star \\ C_z(\rho)G(\rho) & 0 & \gamma_\infty I & \star \\ 0 & B_w^T(\rho) & D_w^T(\rho) & \gamma_\infty I \end{bmatrix} \tag{25}$$

Note that this condition is the same condition as Eq. (A.5), from Lemma 2, when $\mathcal{A}$, $\mathcal{B}$, C and $\mathcal{D}$ are given as in Eq. (22). Applying the Projection Lemma over condition (24) to eliminate the matrix block $K(\rho)$, Eq. (18) is then recovered as an equivalent condition to Eq. (24). This proves that Eq. (18) is a sufficient condition to demonstrate the existence of a State-Feedback control gain $K(\rho)$ such that $\Xi_{CL}(\rho)$ is exponentially stable with induced L_2-norm less than γ_∞. ■

Notice that when applying the projection lemma on (24), it imposes condition (18) and additionally

$$\mathcal{N}_N^T(\rho)\Psi(\rho)\mathcal{N}_N(\rho) > 0, \tag{26}$$

with

$$\mathcal{N}_N(\rho) = \ker\left(\begin{bmatrix} G(\rho) & 0 & 0 & 0 \end{bmatrix} \right). \tag{27}$$

Now equation (27) can be rewritten as (Gahinet and Apkarian, 1994)

$$\begin{aligned}\mathcal{N}_N(\rho) &= \begin{bmatrix} G(\rho)^{-1} & \star & \star & \star \\ 0 & I & \star & \star \\ 0 & 0 & I & \star \\ 0 & 0 & 0 & I \end{bmatrix} \ker\left(\begin{bmatrix} I & 0 & 0 & 0 \end{bmatrix} \right) \\ &:= \hat{G}(\rho)^{-1}\hat{\mathcal{N}}_N(\rho)\end{aligned} \tag{28}$$

Replacing (28) in condition (26) leads to:

$$\begin{aligned}\hat{\mathcal{N}}_N^T(\rho) \Bigg\{ \begin{bmatrix} G(\rho)^{-T} & \star & \star & \star \\ 0 & I & \star & \star \\ 0 & 0 & I & \star \\ 0 & 0 & 0 & I \end{bmatrix} \Psi(\rho) \\ \times \begin{bmatrix} G(\rho)^{-1} & \star & \star & \star \\ 0 & I & \star & \star \\ 0 & 0 & I & \star \\ 0 & 0 & 0 & I \end{bmatrix} \Bigg\} \hat{\mathcal{N}}_N(\rho) > 0\end{aligned} \tag{29}$$

Using Eq. (25), this condition leads to the already known constraint $X(\rho) > 0$. As a result, condition (26) can then be discarded to prove the equivalency between conditions in Eq. (18) and Eq. (24) due to the Projection Lemma, for the case of the SF control problem. This fact is similar to the one seen in *Corollary 1* of (Lu and Wu, 2004), when applying the Projection Lemma over the BRL for the SF case, only the condition involving the null space of $[B_u^T, D_u^T]$ is considered.

3.2. Reduction to a Finite-Dimensional LMI Problem

Theorem 1 provides general conditions to prove the existence of some controller $K(\rho)$ for the control of the DT LPV system $\Xi(\rho)$. However, it is numerically very hard to implement, since it is infinitely constrained as it must hold true $\forall\rho \in \Omega$. Moreover, Eq. (18) requires the knowledge of ρ^+, which again, can take on infinite possible values and imposes an infinite number of constraints. Nonetheless, Theorem 1 can be recasted to a finite number of LMI using the parameter grid and local variation bounds approach explored in Sect. 2.

Note that it is also possible to recast the conditions from Theorem 1 into a numerical solvable LMI problem by using the well known Polyquadratic Polytopic approach (Daafouz and Bernussou, 2001a) for discrete-time systems. However, this approach would imply that the input matrices B_u, D_u of the DT-LPV system in Eq. (1) should be constant or pre-filtered to comply with the parameter space convexity requirement of the Polytopic approach (Apkarian et al., 1995). Moreover, a Polytopic solution is known to be more conservative due the over-bounding issues that come from requiring a convex hull that encloses the parameter space and the

assumption of an infinite rate of variation of the varying parameters, as detailed in Sect. 1.1 and Sect. 1.2 or as illustrated in (Li et al., 2021; Kapsalis et al., 2022). For these reasons and in the spirit of reducing conservatism, it has been decided to use the Gridding approach in this paper.

The following proposition gives a numerically tractable implementation of Theorem 1 that can be efficiently solved with available SDP solvers.

Proposition 1. *Consider a DT-LPV system $\Xi(\rho)$, with parameter space $\Omega \in \mathbb{R}^m$ gridded by a grid space $\mathcal{G} \in \Omega$ and assuming bounded parameter rate of variation $\nu \in \mathbb{R}^m$ such that $\forall g_p \in \mathcal{G}$ there exists a bounding polytope $\mathcal{V}_p$ for g_p^+ with 2^m vertices $g_p^v \in \mathcal{V}_p$, and scalar $\gamma_\infty > 0$. If there exists a symmetric positive-definite PDLM $X(\rho) \in \mathbb{R}^{n_x \times n_x}$, with fixed structure as in Eq.* (11)*, and a set of matrices $\mathbf{G_p} \in \mathbb{R}^{n_x \times n_x}$ such that $\forall (g_p, g_p^v)$ pairs the following condition holds*

$$\mathcal{N}_M^T(\theta_p) \begin{bmatrix} \mathbf{G_p}^T + \mathbf{G_p} - X(\theta_p^v) & \star & \star & \star \\ A(\theta_p)G(\theta_p) & X(\theta_p) & \star & \star \\ C_z(\theta_p)G(\theta_p) & 0 & \gamma_\infty I & \star \\ 0 & B_w^T(\theta_p) & D_w^T(\theta_p) & \gamma_\infty I \end{bmatrix} \mathcal{N}_M(\theta_p) > 0 \quad (30)$$

with

$$X(\theta_p) = \mathbf{X_0} + \sum_{n=1}^{N} \theta_p \mathbf{X_n}, \quad (31)$$

$$X(\theta_p^v) = \mathbf{X_0} + \sum_{n=1}^{N} \theta_p^v \mathbf{X_n}, \quad (32)$$

$$\mathcal{N}_M(\theta_p) = ker(\begin{bmatrix} 0 & B_u^T(\theta_p) & D_u^T(\theta_p) & 0 \end{bmatrix}), \quad (33)$$

then, there exists a SF control gain $K(\rho)$ such that the closed-loop form of $\Xi(\rho)$ is exponentially stable and γ_∞ is an upper bound on its induced L_2-norm.

Proof: Proposition 1 is a direct application of Theorem 1 using the parameter grid and local variation bounds approach detailed in Sect. 2. The varying parameter vector ρ is gridded at fixed points g_p alongside the varying parameter space Ω. At each fix grid point g_p the LPV system $\Xi(\rho)$, with affine dependency on some scheduling signal $\theta(\rho)$, is then frozen as an LTI representation $\Xi(\theta_p)$. Meanwhile, using the maximum rates of parameter variation ν, ρ^+ is bounded at each fixed grid point g_p by a polytope $\mathcal{V}_p$, each vertex of this polytope around g_p defined as g_p^v. This concludes the proof. ■

Remark 2. *According to Definition 3, the control problem objective is the minimization of the induced L_2-norm upper bound γ_∞ of the closed-loop form of $\Xi(\rho)$. However, Theorem 1 and Proposition 1 are given with an arbitrary upper bound γ_∞ for the purpose of generalization. Nonetheless, once Proposition 1 has been implemented, the LMI optimization problem can be solved as the minimization of the induced L_2-norm upper bound γ_∞^* as follows:*

$$\gamma_\infty^* = \min_{\mathbf{X_0},\ldots,\mathbf{X_N},\mathbf{G_p},\gamma_\infty} \gamma_\infty \quad s.t. \ (30) \ \forall (g_p, g_p^v) \quad (34)$$

Due to numerical issues, once an optimal upper bound γ_∞^* is found according to Eq. (34)*, it is convenient to recompute the values of $X_0, \ldots, X_N, G_p$ employing Proposition 1 with fixed $\gamma_\infty = \gamma_\infty^*(1+h)$, where h is a percentage (Poussot-Vassal, 2008).*

Remark 3. *It is hard to determine exactly how dense needs to be the grid space $\mathcal{G} \in \Omega$. An ad-hoc solution is to solve the design LMI problem from Proposition 1, then check if stability and performances holds in a much denser grid (Becker, 1996).*

Remark 4. *Note that in Theorem 1 the slack matrix $G(\rho)$ is assumed to be parameter dependent but its structure is not given. One option is to assume an affine dependency on the scheduling function*

$$G(\rho) = G_0 + \sum_{n=1}^{N} \theta_n(\rho) G_n, \quad (35)$$

as the PDLM $X(\rho)$ in Eq. (11)*. However, given that $G(\rho)$ does not play an important role on the proof of system stability as $X(\rho)$ does, forcing a parametric dependency could lead to a conservative solution. To avoid this conservatism, the slack matrix $G(\rho)$ in Proposition 1 is expressed a set of matrices. This solution assumes a parameter dependency such that*

$$G(\rho) = \sum_{p=1}^{P} \zeta_p(\rho) G_p \quad (36)$$

with

$$\zeta_p(\rho) = \begin{cases} 1, & \text{if } \rho = g_p \\ 0, & \text{otherwise} \end{cases} \quad (37)$$

where P is the total number of grid-points in $\mathcal{G}$. This parameter dependency means that for each grid point g_p there exists a unique constant slack matrix G_p.

3.3. Computation of the PDSF Controller $K(\rho)$

If a valid solution to the LMI problem from Proposition 1 exists, then we obtain numerical candidate values for the PDLM $X(\rho)$ and the slack variable $G(\rho)$. Note that with an existing candidate solution for $X(\rho)$ and $G(\rho)$, applying the Extended DT BRL from Lemma 2 in Appendix A.2 over $\Xi_{CL}(\rho)$ in (22), the BRL now results in an LMI with $K(\rho)$ as the only decision variable.

Let us assume a PDSF controller $K(\rho)$, according to Definition 2, with affine dependency on the scheduling functions θ_n and such that

$$K(\rho) = K_0 + \sum_{n=1}^{N} \theta_n(\rho) K_n \tag{38}$$

The following proposition provides an LMI optimization problem that allows to compute the constant gains $K_0, \ldots, K_N$ for the PDSF controller $K(\rho)$.

Proposition 2. *Consider a DT-LPV system $\Xi(\rho)$, with parameter space $\Omega \in \mathbb{R}^m$ gridded by a grid space $\mathcal{G} \in \Omega$ and assuming bounded parameter rate of variation $\nu \in \mathbb{R}^m$ such that $\forall g_p \in \mathcal{G}$ there exists a bounding polytope $\mathcal{V}_p$ for g_p^+ with 2^m vertices $g_p^v \in \mathcal{V}_p$, and scalar γ_∞. Moreover, consider a given symmetric positive-definite PDLM $X(\rho) \in \mathbb{R}^{n_x \times n_x}$, with fixed structure as in Eq.* (11)*, and a set of matrices $G_p \in \mathbb{R}^{n_x \times n_x}$, both computed as the solutions to Proposition 1. If there exists a PDSF controller $K(\rho) \in \mathbb{R}^{n_u \times n_x}$ given by Eq.* (38) *such that $\forall (g_p, g_p^v)$ pairs the following condition holds*

$$\Psi(\theta_p, \theta_p^v) + He\left(\begin{bmatrix} 0 \\ B_u(\theta_p) \\ D_u(\theta_p) \\ 0 \end{bmatrix} K(\theta_p) \begin{bmatrix} G(\theta_p) & 0 & 0 & 0 \end{bmatrix} \right) > 0 \tag{39}$$

where

$$K(\theta_p) = \mathbf{K_0} + \sum_{n=1}^{N} \theta_p \mathbf{K_n}, \tag{40}$$

$$\Psi(\theta_p, \theta_p^v) = \begin{bmatrix} G^T(\theta_p) + G(\theta_p) - X(\theta_p^v) & \star & \star & \star \\ A(\theta_p)G(\theta_p) & X(\theta_p) & \star & \star \\ C_z(\theta_p)G(\theta_p) & 0 & \gamma_\infty I & \star \\ 0 & B_w^T(\theta_p) & D_w^T(\theta_p) & \gamma_\infty I \end{bmatrix} \tag{41}$$

then the closed-loop form of $\Xi(\rho)$ is exponentially stable and γ_∞ is an upper bound on its induced L_2-norm, with control law given by $u = K(\rho)x$.

Proof: Proposition 2 is a direct application of Lemma 2, with gridding relaxations as seen in Sect. 2 and with the SF control gains of $K(\rho)$ as the only unknown variables on the LMI problem.

Consider the closed-loop dynamics $\Xi_{CL}(\rho)$ as in (22). Applying the Extended DT BRL over $\Xi_{CL}(\rho)$ condition (24) is recovered. With a given symmetric positive-definite matrix $X(\rho)$ and given slack variable $G(\rho)$, assume that there exists a SF control gain $K(\rho)$ such that (24) holds true according to Lemma 2. Applying the parameter grid and local variation bounds approach for relaxations on ρ and ρ^+ in (24), results $\forall (g_p, g_p^v)$ pairs in condition (39). This concludes the proof. ■

Remark 5. *It should be noted that there is no strict requirement for $X(\rho)$ and $K(\rho)$ to share the same parameter dependent structure, although this represents the most straightforward solution. One possible structure for the SF controller could simply be $K = K_0$. This represents computing a constant robust SF controller gain K_0 for the whole parameter space Ω which is obviously very conservative. Nonetheless, this highlights that the PDSF controller* (38) *is in fact a parameter dependent robust controller as the controller gains $K_0, \ldots, K_N$ are fixed $\forall \rho \in \Omega$. For this reason, the choice of the parametric dependent basis function $\theta(\rho)$ in Eq.* (38) *is a very important degree of freedom in the synthesis process to achieve non conservative solutions.*

4. Description and Modelling of the Scaled Autonomous Vehicle Test Platform

4.1. Platform Architecture

The Scaled Autonomous Vehicle (SAV) Test Platform at GIPSA-Lab is a 1:20 scaled vehicle running in a Motion Capture room, see Fig. 2, designed to test control and planning algorithms for autonomous vehicles. The main components of the platform are the Motion Capture System, a remote desktop PC and the SAV RC Car. The Motion Capture system is an infrared Vicon Tracker system, capturing at a $100 H_z$ frequency the position and orientation of the SAV on the track. The SAV is a modified RC Car, equipped with two brushless DC motors for longitudinal traction and a Servo Motor as the steering front wheels actuator. Finally, the remote desktop PC runs the ROS2 software (Macenski et al., 2022) to capture and process all the information from the Vicon Tracker system and car sensors. It also executes the control algorithms that are sent to the car via WiFi.

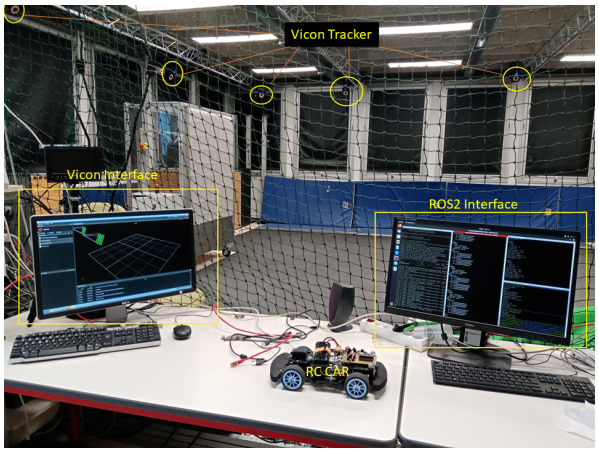

Figure 2: Scaled Autonomous Vehicle Test Platform.

More details on the platform architecture and communications can be seen on Fig. 3. The SAV is controlled by an Arduino RP2040 microcontroller board. The RP2040 board runs microROS, which is used to both receive and send information with the remote PC. The information sent to the remote PC are the IMU measurements, angular speed readings from a dedicated hall-effect encoder for each BLDC motors and the voltage and current measurements from the battery. On the other hand, it receives the set-points commands for the BLDC motors angular speed and Servo Motor steering angle. It should be noted that the RP2040 board acts only as communication transmitter between the onboard sensors/actuators and the remote PC. Specifically, within the scope of this work, the lateral control law is processed remotely and only the communication with the Servo Motor is handled onboard the SAV.

It is the task of the remote PC to handle and process all the data and information coming from the multiple sensors on the platform. The communication layer with the other platform components is handled by the ROS2 software tool by means of subscriptions to the multiple nodes and topics on the software. Importantly, there exist ROS2 libraries that allow to directly access the information from the Vicon mocap system. Whereas the WiFi communication protocol with the SAV is handled automatically by ROS2, the engineering task in this case reduces to subscribing and publishing the information on the ROS2 topics environment. The planning and control algorithm for the SAV are also programmed on the ROS2 environment at the remote PC using Python as the programming language. This is important as it means that the complexity of the algorithms will not be affected by the limited onboard memory and computing power on the SAV.

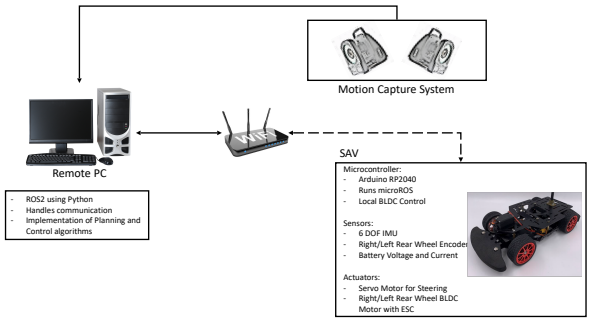

Figure 3: SAV Platform Architecture and Communications.

The Vicon Tracker connects to an interface PC, shown in Fig. 2 as Vicon Interface, which is itself connected with the remote ROS2 PC. The Vicon mocap system works by emitting infrared light, which is reflected by small balls made of infrared reflecting material and which are attached to the SAV. By using multiple infrared cameras, the Vicon system can then detect the position and orientation within the track of the SAV. The position detection by the Vicon system is done with a sub-millimeter accuracy at a frequency of $100H_z$. The precision and low noise from the position and orientation measurement obtained from the mocap system enables smooth and accurate derivation of these signals. As a result, the main signals used for vehicle control, e.g. yaw rate and longitudinal and lateral velocities, are obtained from the derivative of the orientation and position signals from the Vicon system. Note that the signal processing is done remotely on the ROS2 PC.

4.2. Scaled Autonomous Vehicle Dynamical Modelling

In order to design model based control laws to be tested on the SAV, a dynamical model is required. Within the scope of this work, the main interest relies only on the SAV's lateral behaviour. A well-known model to describe the vehicle lateral dynamics is the Bicycle Model (Rajamani, 2011), denoted here $BM(v_x)$ and given by the state-space representation:

$$\begin{bmatrix} \dot{v}_y \\ \ddot{\psi} \end{bmatrix} = \begin{bmatrix} -\frac{C_{af}+C_{ar}}{mv_x} & -v_x - \frac{C_{af}l_f - C_{ar}l_r}{mv_x} \\ -\frac{C_{af}l_f - C_{ar}l_r}{I_z v_x} & -\frac{C_{af}l_f^2 + C_{ar}l_r^2}{I_z v_x} \end{bmatrix} \begin{bmatrix} v_y \\ \dot{\psi} \end{bmatrix} + \begin{bmatrix} \frac{C_{af}}{m} \\ \frac{C_{af}l_f}{I_z} \end{bmatrix} \delta \tag{42}$$

The states of the model are the vehicle lateral velocity v_y and vehicle yaw rate $\dot{\psi}$, both of which are measured on the SAV Platform. The control input of the system is the steering angle at the front wheels δ, which on the

SAV is actuated by the front Servo Motor. However, in practice the control input δ is affected by an input delay due to the WiFi communication delays between the SAV and the Remote PC as well as the processing time to interpret the command signal by the Arduino on board the SAV. For this reason, a better representation for the steering input in Eq. (42) would be $\delta(t-\tau)$, with τ representing a pure input time delay. In the design of the PDSF controller, this input delay will be ignored, in order to evaluate its performance in face of some important unmodeled dynamics.

Note that the model state-space matrices depend on the longitudinal velocity v_x of the vehicle. If the longitudinal velocity is not assumed to be constant, then the Bicycle Model becomes a pure LPV system with v_x as its varying parameter, see Atoui et al. (2022). As in the case of the $BM(v_x)$ states, the longitudinal velocity measurement is also available on the SAV platform. The rest of the model parameters are either measured or identified, with values and description given in Table 1.

Table 1: SAV Bicycle Model Parameters

Parameter	Value	Units	Description
m	1.1937	kg	Vehicle mass
l_f	0.0691	m	COG to front wheels distance
l_r	0.1049	m	COG to rear wheels distance
$C_{\alpha f}$	8.8302	N/rad	Front wheel cornering stiffness
$C_{\alpha r}$	9.7367	N/rad	Rear wheel cornering stiffness
I_z	0.0094	kg/m^2	z Axis Inertia
τ	0.1784	s	Pure input time delay

To identify the non measurable parameters given in Table 1, a non-linear identification was carried. The identification method consits on a Prediction-Error Identification one solving the following non-linear optimization problem (Tóth et al., 2012)

$$\min_{\omega} \|y - \hat{y}(\delta, v_x)\|^2, \tag{43}$$

where y is the stored vector of measurements, in this case both states of the Bicycle Model. $\hat{y}(\delta, v_x)$ is the computed open-loop output of the LPV model (42) with stored input δ and varying parameter v_x. The vector $\omega = [C_{\alpha f}, C_{\alpha r}, I_z, \tau] \in \mathbb{R}^4$ consist of the parameters to identify, which represent the optimization decision variables.

The non-linear identification of the LPV model (42) for the SAV is outside the scope and objectives of this work. However, in order to illustrate the accuracy of the model which will later be used for LPV control design, data from two validations datasets are shown in the following. Figure 4 and Fig. 5 show identification results from a first validation dataset. On the other hand, Fig. 6 and Fig. 7 show identification results from the second validation dataset.

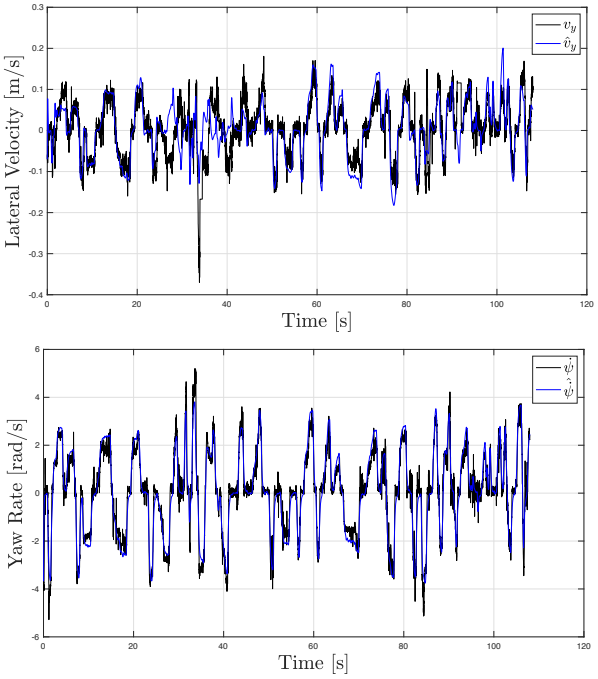

Figure 4: State Measurements and Identified Model Outputs ($\hat{v}_y$,$\hat{\dot{\psi}}$) for the First Validation Dataset.

The first dataset consists of data taken while the SAV was performing smooth maneuvers at high speeds $v_x \in (1, 1.8) m/s$, as can be seen from the information on the steering angle input and longitudinal velocity in Fig. 5. On the other hand, the second dataset was taken while the SAV doing aggressive maneuvers at slow and moderate velocity $v_x \in (0.4, 1.4) m/s$, with information on the abrupt changes on steering angle and the longitudinal velocity in Fig. 7. Both of these datasets are intended to push the limits of the SAV in terms of remaining within the linear range of tire forces, where the assumptions to obtain the LPV model (42) hold (Rajamani, 2011). This can be caused by either aggressive lateral maneuvers or by high longitudinal speed during cornering.

Nonetheless, as can be seen in Fig. 4 and Fig. 6, the output predictions of the identified model captures very well the measured behaviour from the vehicle states. The identified model is specially accurate in predicting the response of the SAV yaw rate measurement, which, as will be seen in the next section, is the signal employed to achieve path tracking of a desired reference trajectory.

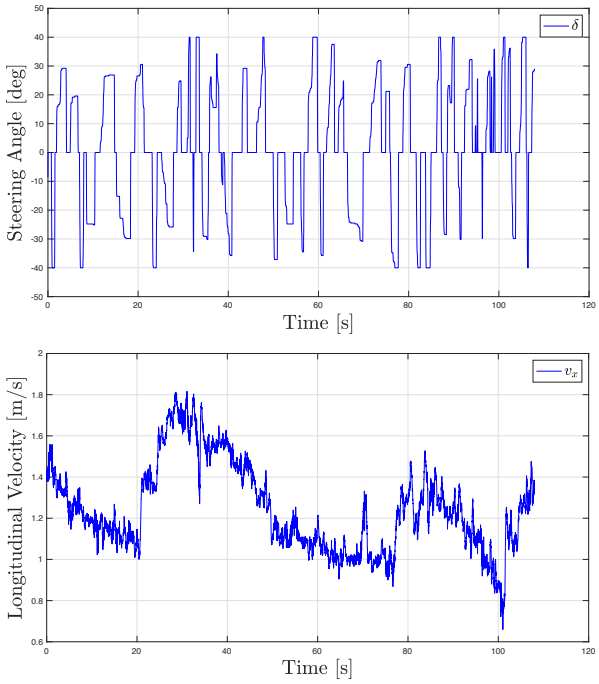

Figure 5: Model input (Up) and Varying Parameter (Bottom) for the First Validation Dataset.

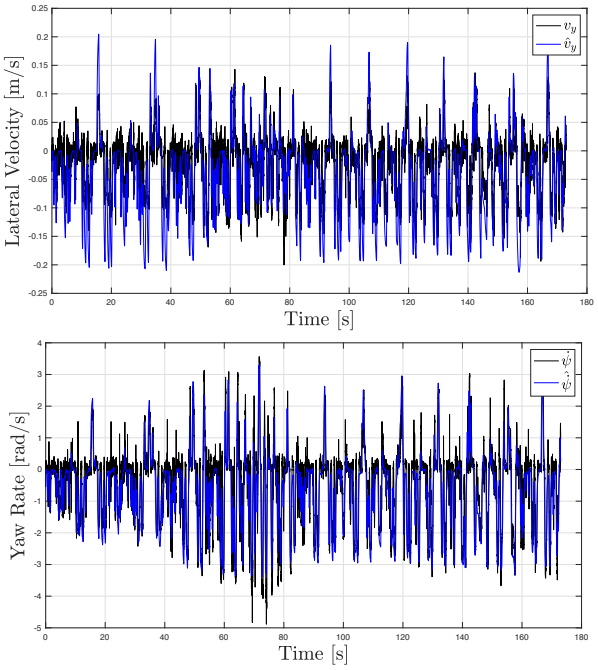

Figure 6: State Measurements and Identified Model Outputs for the Second Validation Dataset.

5. Lateral Control of the Scaled Autonomous Vehicle Using a PDSF Controller

5.1. Reference Generation for Path Tracking

The objective of the control task is to achieve robust path tracking performance of a given trajectory. The trajectory that has been considered for this work is the circuit shown in Fig. 8. The X and Y coordinates that make the circuit have been sampled at $0.01m$ intervals and all the coordinates data points stored as vectors on the Remote PC.

In order to generate the yaw rate reference signal $\dot{\psi}_{ref}$ that will drive the low-level PDSF controller to track the given trajectory, the Pure Pursuit Algorithm is used. This reference generation algorithm has been selected for its simplicity of implementation, good performance and simple tuning with only one parameter to modify (Coulter, 1992; Paden et al., 2016). A brief description of the algorithm is given in the following.

Consider a given configuration of the vehicle $(x, y, \psi)^T$, where x and y are the coordinates of the vehicle on the track and ψ is the heading angle in the inertial frame. Note that all of these variables are available on the SAV platform provided by the Vicon Tracker system. Given a look-ahead distance

$$L = t_p v_x, \tag{44}$$

where t_p is the look-ahead time and v_x the vehicle longitudinal velocity, find a point (x_{ref}, y_{ref}) on the reference trajectory such that $\|(x_{ref}, y_{ref}) - (x, y)\| = L$. Compute the angle α according to

$$\alpha = \arctan\left(\frac{y_{ref} - y}{x_{ref} - x}\right) - \psi \tag{45}$$

Then, the reference yaw rate signal to achieve path tracking is given by

$$\dot{\psi}_{ref} = \frac{2v_x \sin\alpha}{L} \tag{46}$$

Note that the only tuning parameter on the algorithm is the look-ahead time t_p as seen in (44). For this work it has been considered a look-ahead time value of $t_p = 1s$.

5.2. PDSF Control Problem Formulation for Path Tracking on the SAV

In the PDSF controller design process, the first step is to grid the varying parameter, in this case the longitudinal velocity v_x. For control design purpose, it is assumed the following bounds $v_x \in [0.5, 2]m/s$ for the parameter range and $|\nu| \leq 0.02 = a_{max}T_s$ for the maximum rate of parameter variation between consecutive sampling instances, where $a_{max} = 1m/s^2$ is the assumed maximum vehicle acceleration and $T_s = 0.02s$ is the

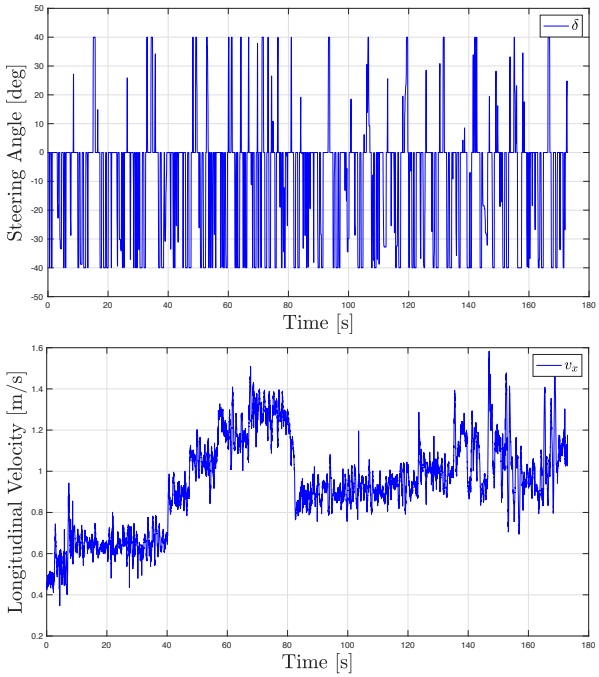

Figure 7: Model input (Up) and Varying Parameter (Bottom) for the Second Validation Dataset.

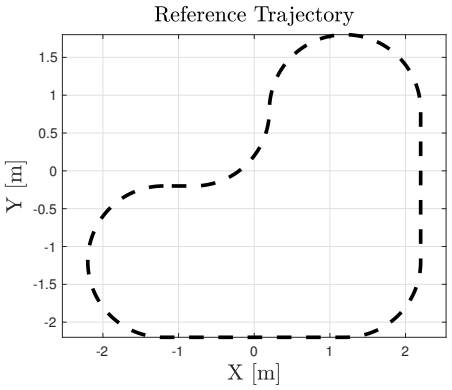

Figure 8: Reference Trajectory.

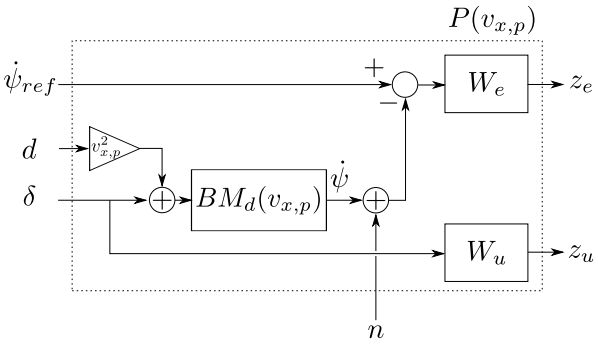

Figure 9: Generalized Plant Scheme at grid-point $v_{x,p}$.

sampling time at which the controller will be implemented. For the gridding space $\mathcal{G}$, the varying parameter v_x has been uniformly gridded at a constant interval of $0.01m/s$. This represents 151 grid-points on the parameter range from $0.5m/s$ to $2m/s$.

From the chosen grid $\mathcal{G}$ of fixed grid-points, at each $v_{x,p}$ we define the reference tracking control problem on the $\mathcal{H}_\infty$ framework by building a generalized plant $P(v_{x,p})$ that includes the weighted performances for tracking and actuator behaviour (Zhou and Doyle, 1998). The chosen scheme for the generalized plant at each grid-point $v_{x,p}$ is given in Fig. 9.

The exogenous inputs of the generalized plant $P(v_x)$ are $w = (\dot{\psi}_{ref}, d, n)^T$. $\dot{\psi}_{ref}$ is the yaw rate reference signal to be followed, d represents an input disturbance and n represents sensor noises in the measurements from the signal $\dot{\psi}$. Note that the input disturbance d at each grid-point is multiplied by the squared value of v_x, e.g. $v_{x,p}^2$. This term is introduced to account for observed disturbance effects on the SAV due to interactions between the lateral dynamics with the longitudinal behaviour, to which the vehicle is more sensitive at higher speeds.

The vector of control performances is $z = (z_e, z_u)^T$, with z_e being the tracking error performance and z_u the actuator performance signal respectively. The used weight W_e to set the tracking specification is the following:

$$W_e = \mathcal{Z}\left(\frac{s/M_s + f_b}{s + f_b\epsilon}\right) \tag{47}$$

Considering $M_s = 2$, $f_b = 2\pi 0.3\ rad/s$ and $\epsilon = 0.01$. Meanwhile, the weight W_u used to specify the constraints on the control signal δ is:

$$W_u = \mathcal{Z}\left(\frac{s + f_{bc}/M_u}{\epsilon_u s + f_{bc}}\right) \tag{48}$$

Considering $M_u = 0.4$, $f_{bc} = 2\pi 10\ rad/s$ and $\epsilon_u = 0.001$. For both weights W_e (47) and W_u (48) the discretization operator $\mathcal{Z}$ has been executed using the Tustin transform.

It is worth noticing the discretized Bicycle Model $BM_d(v_{x,p})$, as seen in Fig. 9, is computed at each of the grid-point $v_{x,p}$ as $BM_d(v_{x,p}) = \mathcal{Z}(BM(v_{x,p}))$, where in this case the $\mathcal{Z}$ operator is executed using a zero-order hold discretization.

Putting all these elements together the generalized plant can be computed for a for a fixed speed grid point $v_{x,p}$ according to the scheme in Fig. 9 with the represen-

tation frozen LTI representation of $P(v_{x,p})$ given by

$$P(v_{x,p}) := \begin{cases} x^+ = A(v_{x,p})x + B_u(v_{x,p})u + B_w(v_{x,p})w \\ z = C_z(v_{x,p})x + D_u(v_{x,p})u + D_w(v_{x,p})w \end{cases} \tag{49}$$

5.3. PDSF Controller Synthesis

With the generalized plant defined at each the grid-point $v_{x,p}$ by Eq. (49), then, the control problem is to find a PDSF controller $K(v_x)$ such that the control law $\delta = K(v_x)x$ minimizes the induced L_2-norm γ_∞ over the generalized plant $P(v_x)$ and controller $K(v_x)$ interconnection, as shown in Fig. 10, such that $\forall v_{x,p} \in \mathcal{G}$

$$\frac{\|z\|_2}{\|w\|_2} \leq \gamma_\infty \tag{50}$$

where $x = (v_y, \dot{\psi}, x_e, x_u)^T$ are the states of the generalized plant $P(v_x)$, with v_y and $\dot{\psi}$ the states of the Bicycle Model (42) and x_e and x_u are the states of the weights W_e and W_u, respectively.

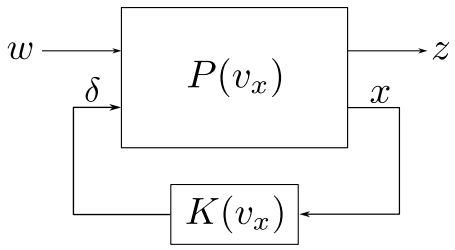

Figure 10: Generalized Plant and controller interconnection.

The existence of such a PDSF controller $K(v_x)$ can then be tested by solving the LMI problem presented in Proposition 1 as a minimization over the scalar γ_∞. The parameter dependent structure that has been assigned for the PDLM $X(\rho)$ for this LMI problem is as follows:

$$X(v_x) = X_0 + \frac{1}{v_x}X_1 + v_x X_2 + v_x^2 X_3 \tag{51}$$

This structure is chosen as it mimics all the ways in which the varying parameter v_x appear in both the generalized plant $P(v_x)$ and correspondingly the Bicycle Model $BM(v_x)$. On the other hand, the parameter dependent slack variable $G(v_x)$ has been chosen such that for each grid-point $v_{x,p}$ there exists a unique slack variable G_p value, as explained in Remark 4.

Using the parser Yalmip (Löfberg, 2004) and the SDPT3 solver (Toh et al., 2004), Proposition 1 can be efficiently solved. It is proved to be feasible with an optimal induced L_2-norm found to be $\gamma_\infty = 10.0184$.

From the solution to Proposition 1, we now have numerical values for the PDLM $X(v_x)$ and the slack matrix $G(v_x)$. Using these values, we can solve Proposition 2 in order to compute the gains of a PDSF controller as seen in Definition 2. With this aim, we select a PDSF controller with the following fixed structure

$$K(v_x) = K_0 + \frac{1}{v_x}K_1 + v_x K_2 + v_x^2 K_3. \tag{52}$$

Employing this choice of structure for the PDSF controller $K(v_x)$, Proposition 2 can be solved with $K_0, \ldots, K_3$ as the only decision variables to be found.

Note that despite having a grid space $\mathcal{G}$ consisting of 151 grid-points, the controller gains in (52) reduces to the four vectors $K_0, \ldots, K_3$, with each $K_n \in \mathbb{R}^4$. In comparison, the usual grid-based LPV approach would require an individual controller gain for each grid-point. Thus, the PDSF controller solution allows to greatly save the memory space that will be required for real-time controller implementation. Moreover, the fact that the number of controller gains is chosen by the control designer through the basis function that forms $K(\rho)$ and not by the number of grid-points, allows one to grid the varying parameter space with a density that simply would not be feasible otherwise for controller synthesis. At the same time, the real-time implementation of the controller $K(v_x)$ is carried by directly implementing Eq. (52) in the software, without requiring any interpolation of point-wise controllers.

5.4. Frequency Analysis of the PDSF Control Design

A first validation of the controller design is carried out on the frequency domain. With this purpose, we consider the closed-loop interconnection between the generalized plant $P(v_x)$ and the PDSF controller $K(v_x)$, as illustrated in Fig. 10, evaluated at some frozen values of the varying parameter $v_{x,p} = (0.5, 0.75, 1, 1.25, 1.5, 1.75, 2) m/s$. Note that this is just small sample of the 151 grid-points used for the synthesis of the PDSF controller. However, it is enough to illustrate the frequency domain response of the closed-loop alongside the whole range of the varying parameter.

In order to validate the yaw rate tracking error $\dot{\psi}_e = \dot{\psi}_{ref} - \dot{\psi}$ response to changes in the yaw rate reference $\dot{\psi}_{ref}$, we compare the sensitivity transfer function $S = \frac{\dot{\psi}_e}{\dot{\psi}_{ref}}$ with respect the employed tracking error template $1/W_e$, with weight W_e given in Eq. (47). Meanwhile, the validation of the constraints of control signal δ response to changes in the yaw rate reference signal $\dot{\psi}_{ref}$ is done by comparing the controller sensitiv-

ity transfer function $KS = \frac{\delta}{\dot{\psi}_{ref}}$ with respect the control action template $1/W_u$, with weight W_u given by Eq. (48). From the frequency response results shown in Fig. 11, it can be seen that both design requirements for the controller $K(v_x)$ are satisfactorily fulfilled for the whole range of values that was consider of the varying parameter v_x in the PDSF design.

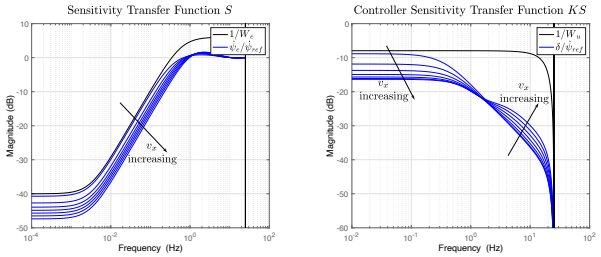

Figure 11: Sensitivity Transfer Function $S = \frac{\dot{\psi}_e}{\dot{\psi}_{ref}}$ versus tracking performance template W_e^{-1} (left) and Controller Sensitivity Transfer Function $KS = \frac{\delta}{\dot{\psi}_{ref}}$ versus actuator performance template W_u^{-1} (right) at frozen values of the varying parameter v_x.

6. Experimental Results

The real-time implementation of the PDSF controller is realized in the remote PC from the SAV test platform. As mentioned previously in Sect. 4, the system states, e.g. v_y and $\dot{\psi}$, as well as the value of the varying parameter v_x are available online from the data measured by the Vicon Tracker. Then, with the gains of the PDSF controller $K(v_x)$ designed and computed as described in Sect. 5.2 and in Sect. 5.3, the control law $\delta = K(v_x)x$ for the SAV steering can be easily implemented on the ROS2 environment of the SAV platform, with $K(v_x)$ given by (52).

The test scenario to demonstrate the path tracking performance of the SAV with PDSF steering controller consists in driving the SAV autonomously on the circuit from Fig. 8 at varying speeds. The speed profile used during the test can be seen in Fig. 12. Recall that the v_x speed profile, shown in Fig. 12, also acts as the varying parameter for the controller $K(v_x)$. Fig. 13 and Fig. 14 present the tracking performance for the reference yaw rate and the control signal, respectively.

Fig. 13 shows in black the yaw rate reference $\dot{\psi}_{ref}$ generated by the Pure Pursuit algorithm, see Sect. 5.1, as the SAV moves through the track, in blue it is given the measured yaw rate by the Vicon Tracker system for the SAV during the test. In Fig. 14, the commanded steering angle δ computed by the PDSF controller $K(v_x)$ is presented.

In order to better visualize the path tracking performance of SAV when using the PDSF controller, Fig. 15 presents information regarding the followed trajectory by the SAV during the test on the X and Y coordinates of the track. On the left of this figure, the reference circuit in black and the trajectory followed by the SAV during the complete test is represented. Note that in order to better identify the multiple laps the SAV has done around the circuit, the followed trajectory is color mapped with the instantaneous longitudinal velocity, corresponding with the information given in Fig. 12. On the right side of this figure, it is given in black the reference trajectory and with blue triangles the orientation and position of the SAV, with the orientation and position taken from a time window of the test from $t \in [40, 50] sec$. Note from Fig. 12 that this time window coincides with a lap made by the SAV at high speeds.

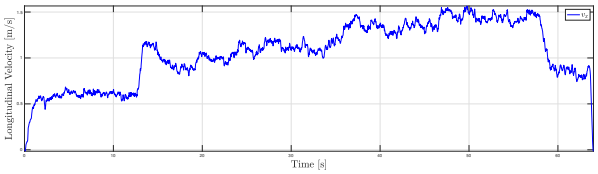

Figure 12: Longitudinal Velocity of the SAV during the test.

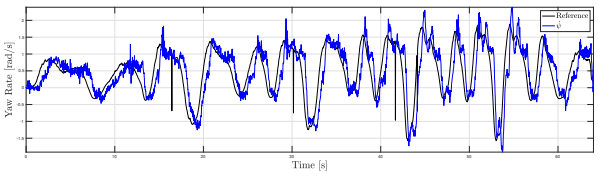

Figure 13: Yaw rate reference (black) and SAV yaw rate (blue) during the test.

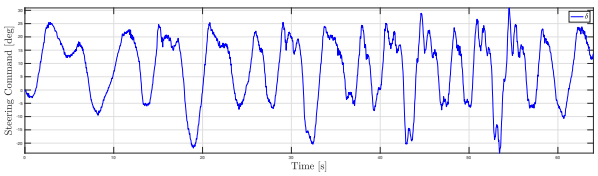

Figure 14: Steering command computed by the PDSF controller.

From the results of the test, we can conclude that with the PDSF controller $K(v_x)$ (52) the SAV achieves very satisfactory path tracking performances. From Fig. 13, it can be seen that the controller is able to track the given reference signal while providing a control signal that is smooth for all the range of speeds seen during the test, as demonstrated by the steering command in Fig. 14. In

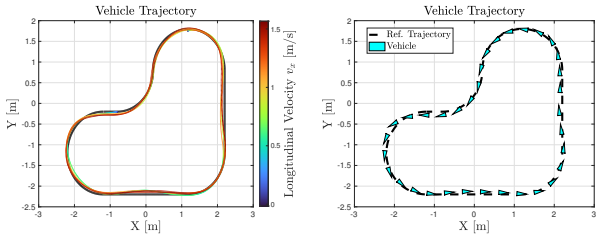

Figure 15: Reference trajectory and actual vehicle trajectory color coded with the instantaneous longitudinal velocity (left). Reference Trajectory and position and orientation of the SAV during a lap done at high speed at $t \in [40, 50] sec$(right).

can be noticed in Fig. 13 the effect of the pure input delay that was ignored during synthesis of the controller. It is well known that unaccounted system delays can lead the closed loop to produce unstable behaviours, despite that, the PDSF controller $K(v_x)$ is able to maintain the vehicle stable and with acceptable reference tracking performance, proving the controller stability in face of critical unmodeled dynamics.

However, it should be noted that at higher speeds, for $t \in [40, 55] sec$, it can be seen in Fig. 13 that some oscillations appear in the yaw rate signal $\dot{\psi}$ after fast changes on the reference. This is a known issue on the platform, caused by the interaction with the longitudinal dynamics of the vehicle due to the behaviour of the dual BLDC motors, which can cause a disturbance torque on the lateral dynamics if their speeds diverge from each other. To attenuate this disturbance effect, higher at larger speeds, it was introduced during the controller design the term $v_{x,p}^2$ on the input disturbance, see Fig. 9.

The tracking performance can specially be verified in Fig. 15 (left). It can be seen how the trajectory of the SAV during multiple laps overlap with each other almost perfectly, even though there exist an important variation in speed during the complete test. This demonstrates that while being very simple to implement, the PDSF controller allows for a consistent performance throughout the considered parameter space for v_x. Moreover on Fig. 15 (right), during the evolution of the SAV position and orientation there is no noticeable evidence of sliding during trajectory even at high speed, meaning that the PDSF controller can cope with demanding situations while keeping the stability of the system.

7. Conclusions

This paper has proposed LMI conditions for the computation of PDSF controllers. Although imposing a parameter dependent structure with fixed gains on the controller could lead to a conservative solution, it has been seen throughout the paper the advantages of the PDSF control approach. First of all, the resulting controller is straightforward to implement as it is self-scheduled based on the imposed parametric basis function (no online interpolation is required) and lightweight on the required memory space. On the other hand, the Parametric LPV synthesis approach allows to use very dense grids on the parameter space without increasing the number of controller gains to be implemented, something which is desirable when using grid-based LPV approaches in order to obtain better stability and performances guarantees.

The performance of this control strategy has been tested on an Scaled Autonomous Vehicle for the task of trajectory tracking showing good path following performances. This has been achieved with a PDSF controller that only required four controller gains to be implemented, despite using 151 grid points for the synthesis step. The found controller provided a satisfactory tracking of the desired reference signal for the whole range of the parameter space of varying parameter. This was achieved in spite of unaccounted model uncertainties as the presence of actuator input delays. Future works could be carried with an emphasis on the SAV application example. These studies can further improve the results for the path following problem use case for which the PDSF controller has been shown here. Moreover, these studies could be used to provide a deep comparison of the PDSF framework introduced in this work with other LPV and control approaches.

Acknowledgments

This work has been supported by the French National Research Agency (CNRS, “Investissements d’Avenir”, ANR-15-IDEX-02) and has been partially supported by ROBOTEX 2.0 (Grants ROBOTEX ANR-10-EQPX-44-01 and TIRREX ANR-21-ESRE-0015) funded by the French program Investissements d’avenir. It has also been partially funded by the Spanish State Research Agency (AEI) and the European Regional Development Fund (ERFD) through the project SaCoAV (ref. MINECO PID2020-114244RB-I00) and by FPI UPC grant 2020FPI-UPC-008.

Appendix A. Useful Literature Results

In this section we collect some existing results and lemmas on the literature which are used for the development of the results presented on this work.

Appendix A.1. Projection Lemma

The following lemma, known as the Projection Lemma or Elimination Lemma in the literature, is the key lemma that allows the computation of Parametric LPV controllers.

Lemma 1 (Projection Lemma)**.** *Given a symmetric matrix $\Psi \in \mathbb{R}^{m\times m}$ and two matrices N, M of column dimension m, consider the problem of finding some matrix Θ of compatible dimensions such that*

$$\Psi + N^T\Theta^T M + M^T\Theta N > 0. \tag{A.1}$$

Denote $\mathcal{N}_M$, $\mathcal{N}_N$ any matrices whose columns form bases of the null spaces of M and N respectively. Then (A.1) *is solvable for Θ if and only if*

$$\begin{cases} \mathcal{N}_M^T\Psi\mathcal{N}_M > 0 \\ \mathcal{N}_N^T\Psi\mathcal{N}_N > 0 \end{cases} \tag{A.2}$$

Appendix A.2. Induced L_2-norm performance

Consider a LPV system:

$$\Xi(\rho) = \begin{cases} x^+ = \mathcal{A}(\rho)x + \mathcal{B}(\rho)w \\ z = C(\rho)x + \mathcal{D}(\rho)w \end{cases} \tag{A.3}$$

where $x \in \mathbb{R}^{n_x}$ is the state vector, $u \in \mathbb{R}^{n_u}$ are the control inputs, $w \in \mathbb{R}^{n_w}$ are the exogenous inputs with bounded energy such that $w \in L_2$ and $z \in \mathbb{R}^{n_z}$ are the exogenous outputs. The induced L_2-norm for $\Xi(\rho)$ is defined as

$$\sup_{w(k)\neq 0} \frac{\|z(k)\|_2}{\|w(k)\|_2} \tag{A.4}$$

An upper bound γ_∞ on the induced L_2-norm of $\Xi(\rho)$ can be computed according to the following Extended Discrete-Time Bounded Real Lemma (DT BRL). Note that extended versions of the DT BRL for time varying systems have been well studied in the literature, see (Daafouz and Bernussou, 2001b; De Caigny et al., 2010; Pandey and de Oliveira, 2019) and references therein.

Lemma 2 (Extended DT Bounded Real Lemma)**.** *If there exists bounded matrices $G(\rho) \in \mathbb{R}^{n_x\times n_x}$ and $X(\rho) = X^T(\rho) > 0$ such that*

$$\begin{bmatrix} G^T(\rho) + G(\rho) - X(\rho^+) & \star & \star & \star \\ \mathcal{A}(\rho)G(\rho) & X(\rho) & \star & \star \\ C(\rho)G(\rho) & 0 & \gamma_\infty I & \star \\ 0 & \mathcal{B}^T(\rho) & \mathcal{D}^T(\rho) & \gamma_\infty I \end{bmatrix} > 0 \tag{A.5}$$

then $\Xi(\rho)$ is exponentially stable and $\frac{\|z(k)\|_2}{\|w(k)\|_2} \leq \gamma_\infty$.

References

Alcalá, E., Puig, V., Quevedo, J., Rosolia, U., 2020. Autonomous racing using linear parameter varying-model predictive control (lpv-mpc). Control Engineering Practice 95, 104270. doi:https://doi.org/10.1016/j.conengprac.2019.104270.

Apkarian, P., Adams, R., 1998. Advanced gain-scheduling techniques for uncertain systems. IEEE Transactions on Control Systems Technology 6, 21–32. doi:10.1109/87.654874.

Apkarian, P., Gahinet, P., 1995. A convex characterization of gain-scheduled h_∞ controllers. IEEE Transactions on Automatic Control 40, 853–864. doi:10.1109/9.384219.

Apkarian, P., Gahinet, P., Becker, G., 1995. Self-scheduled h_∞ control of linear parameter-varying systems: a design example. Automatica 31, 1251–1261. doi:https://doi.org/10.1016/0005-1098(95)00038-X.

Atoui, H., Sename, O., Milanés, V., Martinez, J.J., 2022. Lpv-based autonomous vehicle lateral controllers: A comparative analysis. IEEE Transactions on Intelligent Transportation Systems 23, 13570–13581. doi:10.1109/TITS.2021.3125771.

Baldelli, D.H., Lee, D.H., Pena, R.S.S., Cannon, B., 2008. Modeling and control of an aeroelastic morphing vehicle. Journal of Guidance, Control, and Dynamics 31, 1687–1699. doi:10.2514/1.35445.

Becker, G., 1996. Additional results on parameter-dependent controllers for lpv systems. IFAC Proceedings Volumes 29, 3222–3227. doi:https://doi.org/10.1016/S1474-6670(17)58172-0. 13th World Congress of IFAC, 1996, San Francisco USA, 30 June - 5 July.

Bianchi, F.D., Sánchez-Peña, R.S., 2022. A method for reducing implementation complexity in linear parameter-varying controllers. Automatica 146, 110588. doi:https://doi.org/10.1016/j.automatica.2022.110588.

Boyd, S., El Ghaoui, L., Feron, E., Balakrishnan, V., 1994. Linear Matrix Inequalities in System and Control Theory. Society for Industrial and Applied Mathematics. doi:10.1137/1.9781611970777.

Corno, M., Panzani, G., Roselli, F., Giorelli, M., Azzolini, D., Savaresi, S.M., 2021. An lpv approach to autonomous vehicle path tracking in the presence of steering actuation nonlinearities. IEEE Transactions on Control Systems Technology 29, 1766–1774. doi:10.1109/TCST.2020.3006123.

Coulter, R.C., 1992. Implementation of the pure pursuit path tracking algorithm. Technical Report. Carnegie-Mellon UNIV Pittsburgh PA Robotics INST.

Cox, P.B., Weiland, S., Tóth, R., 2018. Affine parameter-dependent lyapunov functions for lpv systems with affine dependence. IEEE Transactions on Automatic Control 63, 3865–3872. doi:10.1109/TAC.2018.2824982.

Daafouz, J., Bernussou, J., 2001a. Parameter dependent lyapunov functions for discrete time systems with time varying parametric uncertainties. Systems & Control Letters 43, 355–359. doi:https://doi.org/10.1016/S0167-6911(01)00118-9.

Daafouz, J., Bernussou, J., 2001b. Poly-quadratic stability and h_∞ performance for discrete systems with time varying uncertainties, in: Proceedings of the 40th IEEE Conference on Decision and Control (Cat. No.01CH37228), pp. 267–272 vol.1. doi:10.1109/CDC.2001.980110.

De Caigny, J., Camino, J., Oliveira, R., Peres, P., Swevers, J., 2010. Gain-scheduled $\mathcal{H}_2$ and $\mathcal{H}_\infty$ control of discrete-time polytopic time-varying systems. IET Control Theory & Applications 4, 362–380(18).

de Oliveira, M., Bernussou, J., Geromel, J., 1999. A new discrete-time robust stability condition. Systems & Control Letters 37, 261–265. doi:https://doi.org/10.1016/S0167-6911(99)00035-3.

Gahinet, P., Apkarian, P., 1994. A linear matrix inequality approach to

h∞ control. International Journal of Robust and Nonlinear Control 4, 421–448. doi:https://doi.org/10.1002/rnc.4590040403.

Hang, P., Chen, X., 2021. Path tracking control of 4-wheel-steering autonomous ground vehicles based on linear parameter-varying system with experimental verification. Proceedings of the Institution of Mechanical Engineers, Part I: Journal of Systems and Control Engineering 235, 411–423. doi:10.1177/0959651820934572.

Hoffmann, C., Hashemi, S.M., Abbas, H.S., Werner, H., 2012. Closed-loop stability and performance optimization in lpv control based on a reduced parameter set, in: 2012 IEEE 51st IEEE Conference on Decision and Control (CDC), pp. 5146–5151. doi:10.1109/CDC.2012.6427053.

Hoffmann, C., Hashemi, S.M., Abbas, H.S., Werner, H., 2014. Synthesis of lpv controllers with reduced implementation complexity, in: 2014 American Control Conference, pp. 3766–3771. doi:10.1109/ACC.2014.6858716.

Hoffmann, C., Werner, H., 2015. A survey of linear parameter-varying control applications validated by experiments or high-fidelity simulations. IEEE Transactions on Control Systems Technology 23, 416–433. doi:10.1109/TCST.2014.2327584.

Kajiwara, H., Apkarian, P., Gahinet, P., 1999. Lpv techniques for control of an inverted pendulum. IEEE Control Systems Magazine 19, 44–54. doi:10.1109/37.745767.

Kapsalis, D., Sename, O., Milanes, V., Molina, J.J., 2022. A reduced lpv polytopic look-ahead steering controller for autonomous vehicles. Control Engineering Practice 129, 105360. doi:https://doi.org/10.1016/j.conengprac.2022.105360.

Kwiatkowski, A., Werner, H., 2008. Pca-based parameter set mappings for lpv models with fewer parameters and less overbounding. IEEE Transactions on Control Systems Technology 16, 781–788. doi:10.1109/TCST.2007.903094.

Li, P., Lam, J., Lu, R., Li, H., 2022. Variable-parameter-dependent saturated robust control for vehicle lateral stability. IEEE Transactions on Control Systems Technology 30, 1711–1722. doi:10.1109/TCST.2021.3121395.

Li, P., Nguyen, A.T., Du, H., Wang, Y., Zhang, H., 2021. Polytopic lpv approaches for intelligent automotive systems: State of the art and future challenges. Mechanical Systems and Signal Processing 161, 107931. doi:https://doi.org/10.1016/j.ymssp.2021.107931.

Liu, L., Leonhardt, S., Misgeld, B.J.E., 2018. Experimental validation of a torque-controlled variable stiffness actuator tuned by gain scheduling. IEEE/ASME Transactions on Mechatronics 23, 2109–2120. doi:10.1109/TMECH.2018.2854416.

Löfberg, J., 2004. Yalmip : A toolbox for modeling and optimization in matlab, in: In Proceedings of the CACSD Conference, Taipei, Taiwan.

Lu, B., Wu, F., 2004. Control design of switched lpv systems using multiple parameter-dependent lyapunov functions, in: Proceedings of the 2004 American Control Conference, pp. 3875–3880 vol.4. doi:10.23919/ACC.2004.1384517.

López-Estrada, F.R., Rotondo, D., Valencia-Palomo, G., 2019. A review of convex approaches for control, observation and safety of linear parameter varying and takagi-sugeno systems. Processes 7.

Macenski, S., Foote, T., Gerkey, B., Lalancette, C., Woodall, W., 2022. Robot operating system 2: Design, architecture, and uses in the wild. Science Robotics 7, eabm6074. doi:10.1126/scirobotics.abm6074.

Mohammadpour, J., Scherer, C.W., 2012. Control of linear parameter varying systems with applications. Springer US, Boston, MA.

Oliveira, M.C.D., Geromel, J.C., Bernussou, J., 2002. Extended h_2 and h_∞ norm characterizations and controller parametrizations for discrete-time systems. International Journal of Control 75, 666–679. doi:10.1080/00207170210140212.

Paden, B., Čáp, M., Yong, S.Z., Yershov, D., Frazzoli, E., 2016. A survey of motion planning and control techniques for self-driving urban vehicles. IEEE Transactions on Intelligent Vehicles 1, 33–55. doi:10.1109/TIV.2016.2578706.

Pandey, A.P., de Oliveira, M.C., 2019. Discrete-time $\mathcal{H}_\infty$ control of linear parameter-varying systems. International Journal of Control 92, 2750–2760. doi:10.1080/00207179.2018.1459855.

Poussot-Vassal, C., 2008. Robust LPV multivariable Automotive Global Chassis Control. Theses. Institut National Polytechnique de Grenoble - INPG. URL: `https://theses.hal.science/tel-00351472`.

Rajamani, R., 2011. Vehicle dynamics and control. Springer Science & Business Media.

Rizvi, S.Z., Mohammadpour, J., Tóth, R., Meskin, N., 2016. A kernel-based pca approach to model reduction of linear parameter-varying systems. IEEE Transactions on Control Systems Technology 24, 1883–1891. doi:10.1109/TCST.2016.2517126.

Rodrigues, L., Oliveira, R., Camino, J., 2018. Parameterized lmis for robust and state feedback control of continuous-time polytopic systems. International Journal of Robust and Nonlinear Control 28, 940–952. doi:https://doi.org/10.1002/rnc.3911.

Sanjuan, A., Rotondo, D., Nejjari, F., Sarrate, R., 2022. A recursive lmi-based algorithm for efficient vertex reduction in lpv systems. International Journal of Control 95, 3379–3391. doi:10.1080/00207179.2021.1973682.

Sato, M., 2022. From impractical lpv controllers to practical and "implementable" lpv controllers: Verification with research airplane. IFAC-PapersOnLine 55, 73–84. doi:https://doi.org/10.1016/j.ifacol.2022.11.293. 5th IFAC Workshop on Linear Parameter Varying Systems LPVS 2022.

Shamma, J.S., 2012. An overview of lpv systems, in: Mohammadpour, J., Scherer, C.W. (Eds.), Control of Linear Parameter Varying Systems with Applications. Springer US, Boston, MA, pp. 3–26.

Toh, K., Tutuncu, R., Todd, M., 2004. On the implementation of sdpt3 (version 3.1) - a matlab software package for semidefinite-quadratic-linear programming, in: 2004 IEEE International Conference on Robotics and Automation (IEEE Cat. No.04CH37508), pp. 290–296. doi:10.1109/CACSD.2004.1393891.

Tóth, R., Heuberger, P.S.C., Van den Hof, P.M.J., 2012. Prediction-error identification of lpv systems: Present and beyond, in: Mohammadpour, J., Scherer, C.W. (Eds.), Control of Linear Parameter Varying Systems with Applications. Springer US, Boston, MA, pp. 27–58.

Wu, F., Yang, X.H., Packard, A., Becker, G., 1996. Induced l2-norm control for lpv systems with bounded parameter variation rates. International Journal of Robust and Nonlinear Control 6, 983–998. doi:https://doi.org/10.1002/(SICI)1099-1239(199611)6:9/10¡983::AID-RNC263¿3.0.CO;2-C.

Zhou, K., Doyle, J.C., 1998. Essentials of robust control. volume 104. Prentice hall Upper Saddle River, NJ.